Cell Reports
Article

Feedback Regulation of Receptor-Induced Ca^{2+} Signaling Mediated by E-Syt1 and Nir2 at Endoplasmic Reticulum-Plasma Membrane Junctions

Chi-Lun Chang,[1] Ting-Sung Hsieh,[1] T. Tony Yang,[2] Karen G. Rothberg,[3] D. Berfin Azizoglu,[1] Elzibeth Volk,[1] Jung-Chi Liao,[2] and Jen Liou[1,*]
[1]Department of Physiology, UT Southwestern Medical Center, Dallas, TX 75390, USA
[2]Department of Mechanical Engineering, Columbia University, New York, NY 10027, USA
[3]Department of Cell Biology, UT Southwestern Medical Center, Dallas, TX 75390, USA
*Correspondence: jen.liou@utsouthwestern.edu
http://dx.doi.org/10.1016/j.celrep.2013.09.038

SUMMARY

Endoplasmic reticulum (ER)-plasma membrane (PM) junctions are highly conserved subcellular structures. Despite their importance in Ca^{2+} signaling and lipid trafficking, the molecular mechanisms underlying the regulation and functions of ER-PM junctions remain unclear. By developing a genetically encoded marker that selectively monitors ER-PM junctions, we found that the connection between ER and PM was dynamically regulated by Ca^{2+} signaling. Elevation of cytosolic Ca^{2+} triggered translocation of E-Syt1 to ER-PM junctions to enhance ER-to-PM connection. This subsequently facilitated the recruitment of Nir2, a phosphatidylinositol transfer protein (PITP), to ER-PM junctions following receptor stimulation. Nir2 promoted the replenishment of PM phosphatidylinositol 4,5-bisphosphate (PIP_2) after receptor-induced hydrolysis via its PITP activity. Disruption of the enhanced ER-to-PM connection resulted in reduced PM PIP_2 replenishment and defective Ca^{2+} signaling. Altogether, our results suggest a feedback mechanism that replenishes PM PIP_2 during receptor-induced Ca^{2+} signaling via the Ca^{2+} effector E-Syt1 and the PITP Nir2 at ER-PM junctions.

INTRODUCTION

The endoplasmic reticulum (ER) is a membrane-bound organelle found in eukaryotic cells that performs key cellular functions, including lipid synthesis, Ca^{2+} regulation, and protein secretion (Friedman and Voeltz, 2011). To coordinate cellular functions and maintain cell homeostasis, the ER forms membrane junctions with other organelles, including the plasma membrane (PM). At ER-PM junctions, the two heterologous membranes are in close apposition with a gap distance ranging from 10 to 30 nm (Toulmay and Prinz, 2011).

ER-PM junctions are platforms for store-operated Ca^{2+} entry (SOCE) (Carrasco and Meyer, 2011; Liou et al., 2005). SOCE is activated by the direct interaction of the ER Ca^{2+} sensor STIM1 and the PM Ca^{2+} channel Orai1 at ER-PM junctions (Lewis, 2011). In addition, ER-PM junctions are implicated in the transport of phosphatidylinositol (PI) synthesized in the ER to the PM to support phototransduction in *Drosophila* photoreceptor cells (Carrasco and Meyer, 2011; Levine, 2004). During phototransduction, light exposure triggers rhodopsin, a G-protein-coupled receptor, to activate the receptor-induced Ca^{2+} signaling pathway mediated by phospholipase C (PLC). Activated PLC hydrolyzes phosphatidylinositol 4,5-bisphosphate (PIP_2) at the PM to generate diacylglycerol and inositol 1,4,5-trisphosphate (IP_3), which subsequently increases cytosolic Ca^{2+} concentration (Berridge et al., 2000). Genetic evidence suggests that *Drosophila* RdgB, a PI transfer protein (PITP), is important for replenishing PM PIP_2 after hydrolysis (Carrasco and Meyer, 2011). Electron microscopy (EM) studies indicate that RdgB is localized to the subrhabdomeric cisternae, an ER domain in close proximity to the PM, in *Drosophila* photoreceptor cells (Vihtelic et al., 1993).

Because ER-PM junctions are sites for Ca^{2+} regulation and lipid transport, changes in density, size, and gap distance of ER-PM junctions are likely to exert profound effects on these important cellular functions. Recently, extended synaptotagmins E-Syt1/E-Syt2/E-Syt3 and their yeast orthologs tricalbins were shown to mediate ER-to-PM tethering (Giordano et al., 2013; Manford et al., 2012). Nevertheless, the regulation and functions of ER-PM junctions are not well understood due to a lack of methods to specifically monitor these junctions without perturbing their functions in mammalian cells.

Here, we describe a genetically encoded marker for ER-PM junctions. Using this marker, we show that increases in cytosolic Ca^{2+} trigger an enhanced ER-to-PM connection mediated by E-Syt1, which subsequently facilitates the recruitment of Nir2, a mammalian ortholog of *Drosophila* RdgB, to ER-PM junctions to promote PM PIP_2 replenishment following receptor

stimulation. Our results reveal a feedback mechanism at ER-PM junctions that replenishes PM PIP_2 during receptor-induced Ca^{2+} signaling.

RESULTS

A Genetically Encoded Marker Selectively Labels ER-PM Junctions

To investigate the dynamic regulation of ER-PM junctions, we designed a genetically encoded marker that selectively labels ER-PM junctions based on the subcellular targeting mechanisms of STIM1. STIM1 is a single transmembrane ER protein that localizes with its N terminus in the ER lumen and C terminus in the cytosol (Figure 1A). We first generated a construct containing the signal peptide (SP) and the transmembrane (TM) domain of STIM1 at the N and C termini, respectively, of a GFP. This SP-GFP-TM fusion protein was localized to the ER (Figure S1A). Next, an FKBP12-rapamycin binding (FRB) domain was added after the TM domain. The addition of FRB domain did not alter the localization (Figure S1B) and may be used to recruit FKBP-fusion proteins using rapamycin or its analogs (Putyrski and Schultz, 2012). STIM1 targeting to ER-PM junctions requires ER Ca^{2+}-depletion-induced oligomerization and a subsequent binding of the C-terminal polybasic motif to phosphoinositides at the PM (Korzeniowski et al., 2009; Liou et al., 2007; Walsh et al., 2010). To enable a constitutive localization to ER-PM junctions, the polybasic motif of the small G protein Rit, which binds to phosphoinositides in the PM (Heo et al., 2006), was added to the C terminus of the marker. We further included several flexible and helical linkers in the cytosolic portion of the marker to ensure that expression of the marker did not alter the gap distance of ER-PM junctions, which range from 10 to 25 nm based on EM studies of mammalian cells (Wu et al., 2006). We named this genetically encoded marker "MAPPER" for "*m*embrane-*a*ttached *peri*pheral *ER*" (Figure 1A).

When MAPPER-transfected HeLa cells were examined using confocal microscopy, hundreds of bright puncta were observed near the adhesion surface of each cell (Figures 1B and S1C). Confocal midsections of MAPPER-transfected cells showed weak signals in the bulk of the ER and nuclear membrane and strong signals in puncta along the cell periphery (Figure S1D). These results indicate that MAPPER is an ER protein highly concentrated at ER-PM junctions similar to activated STIM1. When the localization of MAPPER and an ER luminal marker were examined in the same cells by confocal microscopy, they appeared dramatically different (Figure 1B). Nonetheless, all puncta detected by MAPPER were overlaid with the ER marker, indicating that MAPPER puncta are part of the ER. The overlay of MAPPER and the ER marker was better illustrated using total internal reflection fluorescence (TIRF) microscopy (Figure 1C), which selectively illuminates fluorescence within 100 nm of the PM (Steyer and Almers, 2001). Compared with the ER marker, MAPPER greatly enhanced the identification of ER-PM junctions with minimal background signal from the rest of the ER. We further performed immunogold labeling using an antibody against GFP and observed by EM that MAPPER was highly enriched in regions closely apposed to the PM (Figure 1D). Moreover, a direct labeling of MAPPER by miniSOG, a genetically encoded tag for EM (Shu et al., 2011), resulted in strong electron-dense signals in PM-attached ER regions that are connected to the moderately labeled ER network (Figure 1E). Together, these results demonstrate that we have successfully generated a marker for selective visualization of ER-PM junctions in live and fixed cells using various imaging approaches.

Furthermore, we observed that STIM1 translocated into ER-PM junctions prelabeled by MAPPER following ER Ca^{2+} depletion induced by thapsigargin (TG) (Figure 1F). Consistently, normal SOCE was detected in MAPPER-expressing cells (Figure 1G). We also found that the density of ER-PM junctions detected by MAPPER was similar to that measured by quantifying stable ER puncta detected in cells transfected with the ER marker using TIRF microscopy (Figure 1H). These results indicate that MAPPER monitors ER-PM junctions with minimal perturbations and is thus suitable for investigating the regulation and functions of ER-PM junctions.

ER-PM Junctions Are Dynamically Regulated during Ca^{2+} Signaling

Previous EM studies showed that TG treatment increased the percentage of the PM in close contact with the ER in HeLa and Jurkat cells, suggesting that ER-to-PM connection can be regulated during Ca^{2+} signaling (Orci et al., 2009; Wu et al., 2006). We applied MAPPER to examine the dynamic regulation of ER-PM junctions in live cells and detected a marked increase in MAPPER signal following TG treatment using TIRF microscopy (Figure 2A; Movie S1). Similar increases in MAPPER signal were found in cells treated with histamine (Figure S2A), which stimulates G-protein-coupled histamine receptors and activates Ca^{2+} signaling. The increased MAPPER signal was not a result of cell movement or a focus drift, because no increase was detected by the PM marker cotransfected into the same cells (Figures 2A and S2A). Further analyses revealed a significant increase in density of ER-PM junctions detected by MAPPER (Figure 2B), indicating that new junctions are formed during Ca^{2+} signaling. Interestingly, a significant increase in intensity of preexisting ER-PM junctions was also detected following TG treatment (Figure 2C). These increases were not caused by expression of MAPPER or an increased recruitment of MAPPER to ER-PM junctions because similar increases in density and intensity of stable ER puncta were detected by TIRF microscopy in cells transfected with the ER marker after TG treatment (Figure S2B; Movie S2).

We then tested a hypothesis that the intensity increase was due to an increase in size of single ER-PM junctions, which is between 100 and 200 nm based on EM studies (Orci et al., 2009; Wu et al., 2006). Because the resolution of TIRF microscopy is limited to ~250 nm, we employed a superresolution imaging technique, stimulated emission depletion (STED) microscopy (Willig et al., 2006), to track TG-induced changes in single ER-PM junctions in live cells. We found that the sizes and shapes of single ER-PM junctions labeled by MAPPER remained similar before and after TG treatment (Figures S3A and S3B). We further quantified the lengths of the long and short axes of individual ER-PM junctions by performing double Gaussian fitting (Figure S3C). Before TG treatment, the long and short axes were 272.7 ± 49.5 nm and 176.1 ± 22.5 nm, respectively. No significant

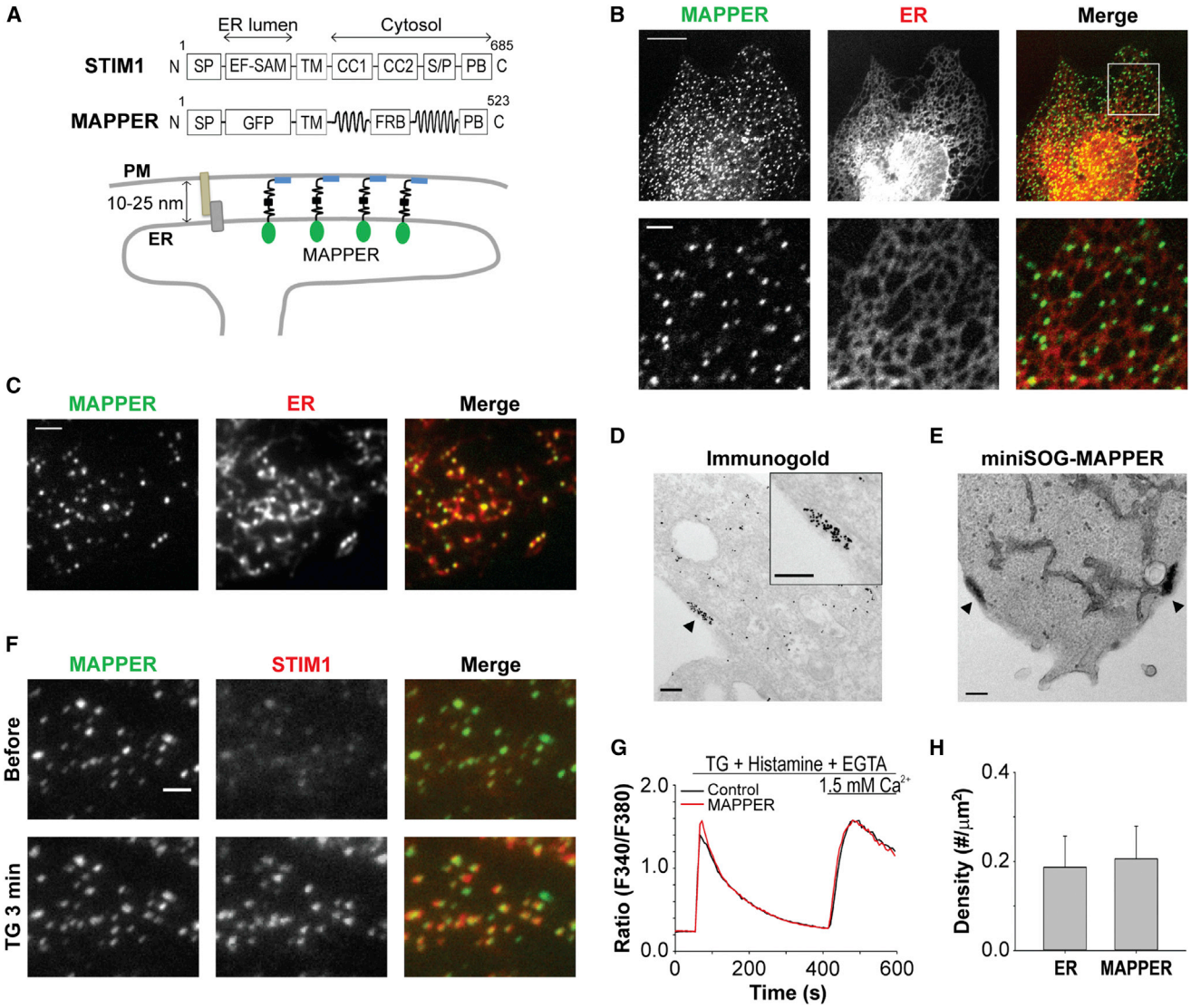

Figure 1. MAPPER Selectively Labels ER-PM Junctions

(A) Diagrams of STIM1 (top) and MAPPER (middle) and a schematic depicting the expected localization of MAPPER at ER-PM junctions maintained by unknown structural components (bottom). Amino acid numbers are indicated. SP, signal peptide; EF-SAM, EF hand and sterile alpha motif; TM, transmembrane; CC1 and CC2, coiled coil domain 1 and 2; S/P, serine and proline rich region; PB, polybasic; FRB, FKBP12-rapamycin binding.

(B) (Top panels) Bottom-section confocal images of a HeLa cell coexpressing MAPPER and mCherry-ER. The scale bar represents 10 μm. (Bottom panels) Magnified images. The scale bar represents 2 μm. See also Figures S1A–S1D.

(C) TIRF images of a HeLa cell coexpressing MAPPER and mCherry-ER. The scale bar represents 2 μm.

(D and E) Ultrastructural analysis of MAPPER localization by EM. (D) Immunogold staining of a MAPPER-transfected cell. The scale bar represents 200 nm. (E) EM image of a HeLa cell transfected with miniSOG-tagged MAPPER. Arrowheads indicate ER-PM junctions. The scale bar represents 200 nm.

(F) STIM1 translocation induced by 1 μM TG monitored by TIRF microscopy in a HeLa cell coexpressing MAPPER and mCherry-STIM1. The scale bar represents 2 μm.

(G) SOCE triggered by 1 μM TG and 100 μM histamine in control (SP-GFP-TM) or MAPPER-transfected HeLa cells. Shown are average traces derived from more than 90 cells.

(H) Density of ER-PM junctions labeled by the ER marker or MAPPER in HeLa cells monitored by TIRF microscopy. Mean ± SD is shown (26 cells from three independent experiments).

changes were detected following TG treatment (Figure S3D). These results suggest that the sizes and shapes of ER-PM junctions are not regulated during Ca^{2+} signaling.

TIRF microscopy is extremely sensitive to changes in distance between a fluorescent protein and the PM (Steyer and Almers, 2001). Because MAPPER contains a GFP in the ER lumen, we hypothesized that the intensity increase induced by TG results from a decrease in gap distance of ER-PM junctions. The gap distance of ER-PM junctions in mammalian cells ranges from 10 to 25 nm (Wu et al., 2006). To test this hypothesis, we

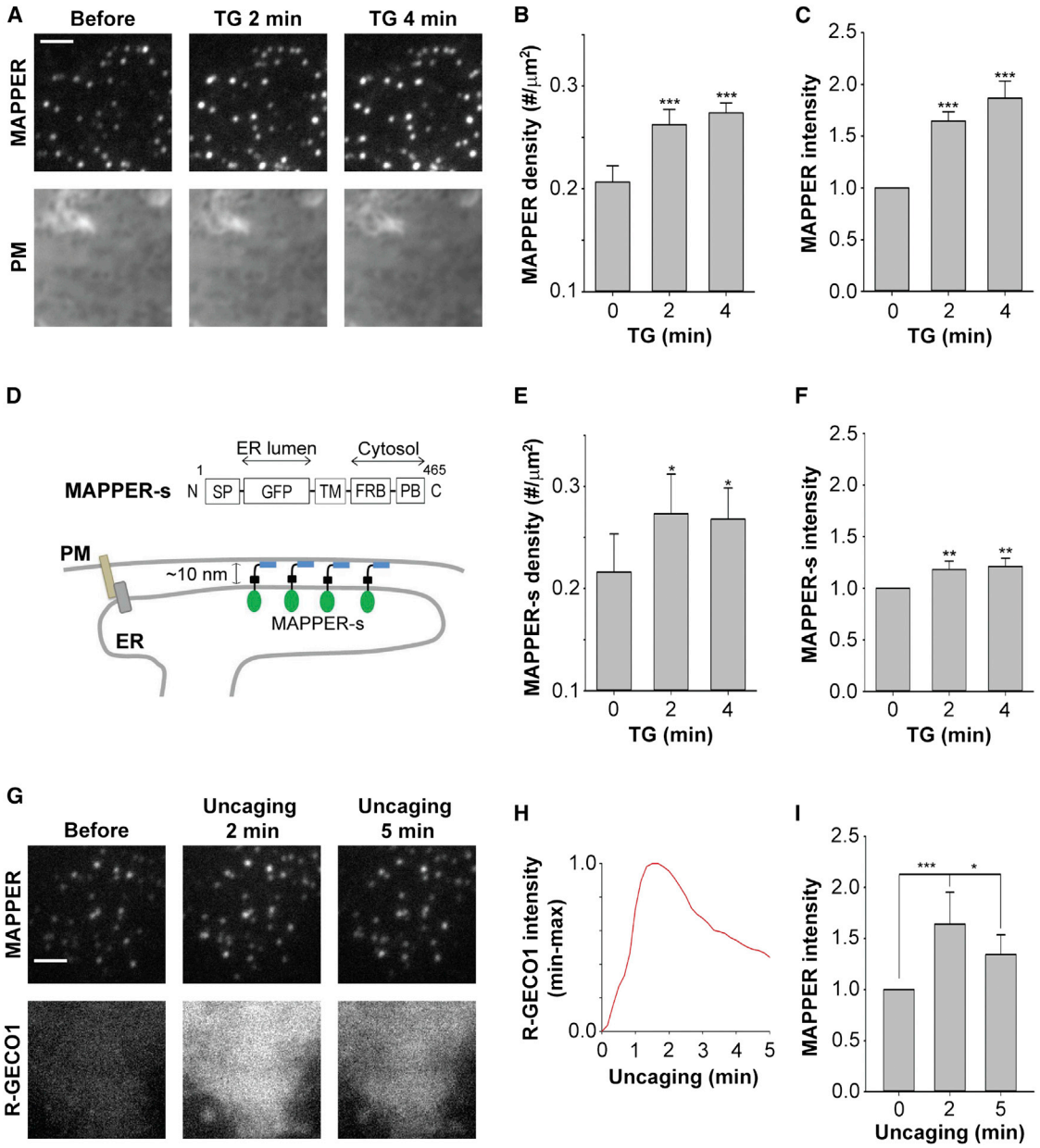

Figure 2. Elevation of Cytosolic Ca^{2+} Enhances ER-to-PM Connection

(A) Dynamic changes in ER-PM junctions induced by 1 μM TG monitored by TIRF microscopy in MAPPER-expressing HeLa cells transfected with a PM marker. The scale bar represents 2 μm. See also Figures S2A and S2B and Movies S1 and S2.

(B and C) Quantification of the dynamic changes in density (B) and intensity (C) of ER-PM junctions monitored as described in (A). Mean ± SD is shown (three to eight cells from at least three independent experiments). The triple asterisks denote $p < 0.001$.

(D) Diagram of MAPPER-s (top) and a schematic depicting how MAPPER-s restricts the gap distance of labeled ER-PM junctions (bottom).

(E and F) Quantification of the dynamic changes in density (E) and intensity (F) of ER-PM junctions induced by 1 μM TG monitored by TIRF microscopy in HeLa cells transfected with MAPPER-s. Mean ± SD is shown (four to six cells from two independent experiments). The asterisk denotes $p < 0.05$ and double asterisks denote $p < 0.01$. See also Figure S2C.

(G) Dynamic changes in ER-PM junctions and R-GECO1 intensities monitored by TIRF microscopy during UV-induced Ca^{2+} uncaging in MAPPER-expressing HeLa cells transfected with R-GECO1 and loaded with NP-EGTA. The scale bar represents 2 μm. See also Figures S4A–S4D and Movie S3.

(H) Relative changes in R-GECO1 intensity monitored as described in (G). Shown is the average R-GECO1 intensity trace (five cells from two independent experiments).

(I) Dynamic changes in intensity of ER-PM junctions monitored as described in (G). Mean ± SD is shown (seven cells from two independent experiments). The asterisk denotes $p < 0.05$ and triple asterisks denote $p < 0.001$.

generated MAPPER-s, which contains a shorter cytosolic region than MAPPER, thus restricting the range of gap distance of labeled ER-PM junctions to ~10 nm or less (Figure 2D). Following TG stimulation, an increase in density of ER-PM junctions similar to that in MAPPER-transfected cells was observed in MAPPER-s-transfected cells (Figures 2E and S2C). However, TG-induced increase in intensity of MAPPER-s-labeled ER-PM junctions was significantly less than in MAPPER-labeled junctions (Figures 2F and S2C). These results imply that the TG-induced increase in MAPPER intensity reflects a decrease in gap distance of ER-PM junctions. Together, our data suggest that treatment with either TG or histamine induces an enhanced ER-to-PM connection by triggering junction formation and by shortening the gap between the ER and the PM.

Elevation of Cytosolic Ca^{2+} Enhances the Connection between the ER and the PM

To dissect the molecular mechanisms underlying the enhanced ER-to-PM connection following TG or histamine treatment, we first tested whether an increase in cytosolic Ca^{2+} was required for the enhanced connection. We found that TG-induced increase in density and intensity of MAPPER-labeled ER-PM junctions was abolished in cells preloaded with BAPTA, a cytosolic Ca^{2+} chelator (phase I and II; Figures S4A–S4D). When 10 mM Ca^{2+} was added to cells to overcome chelation by BAPTA, an elevation in cytosolic Ca^{2+} was accompanied by a dramatic increase in intensity and density of ER-PM junctions (phase III and IV; Figures S4A–S4D; Movie S3). These results demonstrate that the enhanced ER-to-PM connection induced by TG is dependent on an increase in cytosolic Ca^{2+}.

We then tested whether an increase in cytosolic Ca^{2+} alone was sufficient to promote ER-to-PM connection. Cells were cotransfected with MAPPER and R-GECO1, a genetically encoded Ca^{2+} indicator (Zhao et al., 2011), and loaded with NP-EGTA, a photolabile Ca^{2+} chelator. Ca^{2+} uncaging by UV illumination resulted in a transient increase in cytosolic Ca^{2+} as indicated by changes in intensity of R-GECO1 (Figures 2G and 2H). A transient increase with similar kinetics in intensity of MAPPER-labeled ER-PM junctions was also observed (Figures 2G and 2I). These results indicate that the connection between the ER and the PM is dynamically controlled by cytosolic Ca^{2+} levels.

Elevation of Cytosolic Ca^{2+} Induces E-Syt1 Translocation to ER-PM Junctions

Because elevation of cytosolic Ca^{2+} alone is sufficient to enhance ER-to-PM connection, it is plausible to assume the existence of a cytosolic Ca^{2+} sensor that promotes ER-to-PM connection. Recent studies showed that E-Syt1/E-Syt2/E-Syt3 and the tricalbins, a family of C2 domain-containing proteins capable of binding to Ca^{2+} and phospholipids, are localized to ER-PM junctions and contribute to ER-to-PM tethering (Giordano et al., 2013; Manford et al., 2012; Toulmay and Prinz, 2012). E-Syt1 is distinct from E-Syt2 and E-Syt3 as it contains two additional C2 domains. Moreover, E-Syt1 is evenly expressed in all tissues, whereas the expression of E-Syt2 and E-Syt3 is more restricted (Min et al., 2007).

We hypothesized that the dynamic regulation of ER-PM junctions is a universal process and thus tested whether the widely expressed E-Syt1 is the Ca^{2+} sensor that promotes ER-to-PM connection. Consistent with previous findings (Giordano et al., 2013; Min et al., 2007), we observed that E-Syt1, tagged with mCherry at either the N or the C terminus, was localized to the ER in resting cells (Figures S5A and S5G). Remarkably, TG treatment induced E-Syt1 translocation into puncta (Figure S5A; Movie S4), which were subsequently identified as ER-PM junctions in cells cotransfected with MAPPER and E-Syt1 (Figure S5B).

To test whether an increase in cytosolic Ca^{2+} was sufficient to induce E-Syt1 translocation, NP-EGTA was loaded into cells cotransfected with mCherry-E-Syt1 and GEM-GECO1, a genetically encoded Ca^{2+} indicator (Zhao et al., 2011). UV-induced uncaging of NP-EGTA triggered an increase in cytosolic Ca^{2+} that was followed by E-Syt1 translocation to ER-PM junctions (Figure S5C and S5D). The kinetic coupling between cytosolic Ca^{2+} increase and E-Syt1 translocation to ER-PM junctions was clearly illustrated in cells treated with histamine, which induced Ca^{2+} oscillation and the accompanying reversible translocation of E-Syt1 (Movie S5). We further mutated the key aspartic acid residues to alanine in the likely Ca^{2+} binding loops of C2A and C2C domains to generate the corresponding E-Syt1-D406A and E-Syt1-D724A mutants (Min et al., 2007). Following TG treatment, the E-Syt1-D406A mutant translocated to ER-PM junctions (Figure S5E), whereas no translocation of the E-Syt1-D724A mutant was observed (Figure S5F). Similar results were obtained following uncaging of NP-EGTA (Figures S5G–S5I). These observations indicate that E-Syt1 senses elevation of cytosolic Ca^{2+} via its C2C domain and that Ca^{2+} binding is important for E-Syt1 translocation to ER-PM junctions. These results are consistent with the data shown in a report published very recently (Giordano et al., 2013).

Enhanced ER-to-PM Connection Is Mediated by E-Syt1 Translocation to ER-PM Junctions

We further observed that TG-induced increase in ER-to-PM connection, as indicated by the intensity increase of MAPPER-labeled ER-PM junctions, was greatly diminished in cells transfected with small interfering RNA (siRNA) targeting either the 3′ UTR (siE-Syt1_3′ UTR) or the coding sequence of *E-Syt1* (siE-Syt1_cds) compared to cells transfected with control siRNA (siControl) (Figures 3A, 3B, S6A, and S6B). Expression of mCherry-E-Syt1 rescued the defective regulation of ER-PM junctions in cells treated with siE-Syt1_3′ UTR (Figure 3C). These results suggest that E-Syt1 mediates the enhanced ER-to-PM connection during Ca^{2+} signaling. Moreover, expression of the E-Syt1-D724A mutant, which neither senses Ca^{2+} nor translocates to ER-PM junctions, failed to rescue the defective enhanced ER-to-PM connection in siE-Syt1_3′ UTR-treated cells (Figures 3D and 3E). These results indicate that E-Syt1 translocation to ER-PM junctions promotes the connection between the ER and the PM.

Nir2 Translocates to ER-PM Junctions and Promotes PIP_2 Replenishment after Receptor Stimulation

We hypothesized that the enhanced ER-to-PM connection by E-Syt1 facilitates cellular functions at ER-PM junctions during Ca^{2+} signaling. Ca^{2+} signaling is generally triggered by

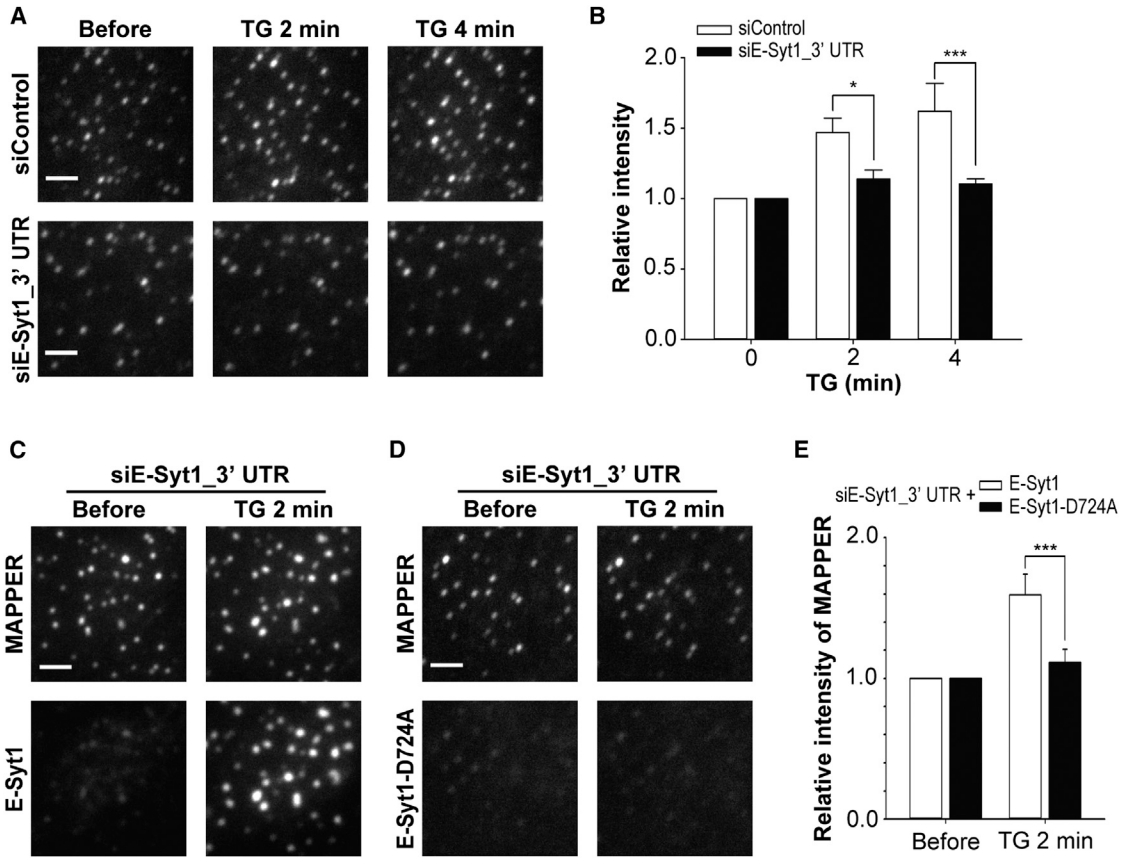

Figure 3. Enhanced ER-to-PM Connection during Ca^{2+} Signaling Is Mediated by E-Syt1 Translocation to ER-PM Junctions

(A) Dynamic changes in ER-PM junctions induced by 1 μM TG monitored by TIRF microscopy in MAPPER-expressing HeLa cells transfected with siControl or siE-Syt1_3′ UTR. The scale bar represents 2 μm. See also Figures S6A and S6B.

(B) Quantification of the dynamic changes in intensities of ER-PM junctions monitored as described in (A). Mean ± SD are shown (four to six cells from at least three independent experiments). The asterisk denotes $p < 0.05$ and triple asterisks denote $p < 0.001$.

(C and D) Dynamic changes in ER-PM junctions and E-Syt1 translocation induced by 1 μM TG monitored by TIRF microscopy in MAPPER-expressing HeLa cells cotransfected with siE-Syt1_3′ UTR and mCherry-E-Syt1 or mCherry-E-Syt1-D724A. The scale bar represents 2 μm.

(E) Quantification of the dynamic changes in intensity of ER-PM junctions monitored as described in (C) and (D). Mean ± SD is shown (four to six cells from three independent experiments). Triple asterisks denote $p < 0.001$.

receptor-induced PLC activation and PM PIP_2 hydrolysis (Berridge et al., 2000). RdgB, a PITP implicated in replenishing PM PIP_2, has been shown to localize to ER-PM junctions in *Drosophila* photoreceptor cells (Carrasco and Meyer, 2011). To test a hypothesis that the enhanced ER-to-PM connection facilitates PM PIP_2 replenishment at ER-PM junctions during Ca^{2+} signaling, we first examined whether Nir2 (also known as PITPNM1), a mammalian ortholog of *Drosophila* RdgB, is localized to ER-PM junctions. We found that a mCherry-tagged Nir2 was localized in the cytosol (Figure 4A). Strikingly, histamine stimulation induced Nir2 translocation into puncta in HeLa cells overexpressing histamine H1 receptor (Figure 4A; Movie S6). We then cotransfected cells with Nir2 and MAPPER and confirmed that Nir2 translocates to ER-PM junctions after histamine stimulation (Figure 4B).

Next, we examined whether Nir2 is involved in replenishing PM PIP_2 after receptor-induced hydrolysis. PIP_2 levels at the PM were monitored using TIRF microscopy and GFP-PLCδ-PH, a PIP_2 biosensor (Stauffer et al., 1998), in HeLa cells overexpressing H1 receptor to augment PIP_2 hydrolysis induced by histamine stimulation. In siControl-transfected cells, a sharp decrease of PLCδ-PH intensity at the PM was observed following histamine stimulation (Figure 4C), reflecting PIP_2 hydrolysis. This decrease was followed by a partial recovery, indicating replenishment of PIP_2 at the PM. Notably, in cells treated with siRNA targeting *Nir2* (siNir2), PIP_2 replenishment was reduced compared to siControl-transfected cells. In contrast, overexpression of Nir2 strongly enhanced PIP_2 replenishment after hydrolysis compared with control-transfected cells (Figure 4D). Similar results were observed using Tubby-GFP (Figure S7A), another biosensor that binds PIP_2 selectively (Quinn et al., 2008). These results indicate that Nir2 mediates PM PIP_2 replenishment after receptor-induced hydrolysis.

PI Transfer Activity and Targeting to ER-PM Junctions Are Important for Nir2 to Promote PIP_2 Replenishment following Receptor Stimulation

The PITP domain of Nir2 has been shown to bind PI in vitro and contains the key residues that make hydrogen bond contact

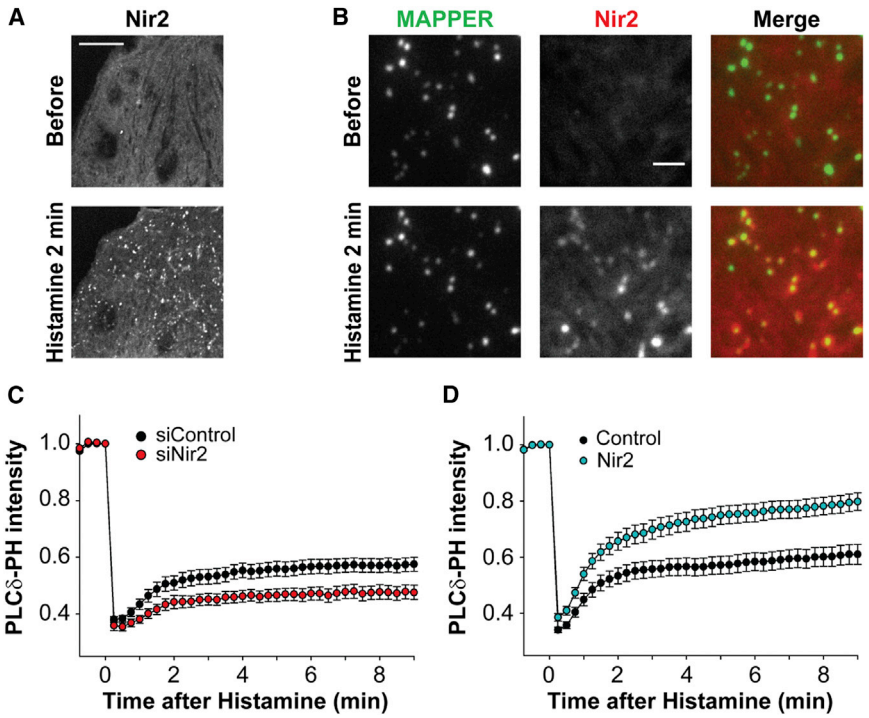

Figure 4. Nir2 Translocates to ER-PM Junctions and Promotes PIP_2 Replenishment following Receptor Stimulation

(A) Nir2 translocation induced by 100 μM histamine monitored by confocal microscopy in HeLa cells cotransfected with H1 receptor and Nir2-mCherry. The scale bar represents 10 μm. See also Movie S6.

(B) Nir2 translocation to ER-PM junctions induced by 100 μM histamine monitored by TIRF microscopy in MAPPER-expressing HeLa cells transfected with H1 receptor and Nir2-mCherry. The scale bar represents 2 μm.

(C) Dynamic changes of PLCδ-PH intensity induced by 100 μM histamine monitored by TIRF microscopy in HeLa cells cotransfected with H1 receptor, GFP-PLCδ-PH, and siControl or siNir2. Mean ± SEM is shown (6–17 cells from three independent experiments).

(D) Dynamic changes of PLCδ-PH intensity induced by 100 μM histamine monitored by TIRF microscopy in HeLa cells cotransfected with H1 receptor, GFP-PLCδ-PH, and control (mCherry-N1 vector) or Nir2-mCherry. Mean ± SEM is shown (25 cells from six independent experiments). See also Figure S7A.

with the inositol head group for the PI transfer activity (Aikawa et al., 1999; Cockcroft, 2012). To test whether the PI transfer activity is required for Nir2 to mediate PIP_2 replenishment, we mutated two of the key residues to generate the Nir2-K61A,N90F mutant. Similar to wild-type Nir2, the Nir2-K61A,N90F mutant was recruited to ER-PM junctions following histamine treatment (Figure 5A). Nevertheless, it failed to promote PIP_2 replenishment (Figure 5B). Similar results were obtained with the Nir2-T59E,N90F mutant (Figures S7B and S7C), and the PITP domain deleted Nir2-ΔPITP mutant (Figures 5C and 5D). These results indicate that a functional PITP domain is essential for Nir2 to promote PM PIP_2 replenishment but is not required for Nir2 recruitment to ER-PM junctions following receptor stimulation.

The translocation of Nir2 from the cytosol to ER-PM junctions suggests that it binds to the ER and the PM simultaneously following receptor stimulation. Nir2 has been shown to interact with the ER membrane proteins VAMP-associated protein A (VAP-A) and VAP-B via its FFAT motif (Amarilio et al., 2005). We observed an accumulation of VAP-A and VAP-B colocalizing with Nir2 at ER-PM junctions following receptor stimulation (Figures 5E and S7D). These results indicate that VAP-A and VAP-B support Nir2 recruitment to ER-PM junctions. We then generated a FFAT mutant of Nir2 (Nir2-FM) that cannot bind VAP proteins as described previously (Amarilio et al., 2005). Nir2-FM was recruited to the PM but failed to concentrate at ER-PM junctions following receptor stimulation, as observed by TIRF microscopy (top panels, Figures 5F and S7E). Consistently, the accumulation of VAP-A and VAP-B at ER-PM junctions was not detected following receptor stimulation (bottom panels, Figures 5F and S7E). These observations suggest that receptor stimulation induces concurrent PM targeting and VAP binding of Nir2, leading to the simultaneous recruitment of Nir2 and VAPs to ER-PM junctions.

Nir2-FM contains a functional PITP domain and targets to the PM instead of ER-PM junctions following receptor stimulation. Interestingly, comparing with cells overexpressing wild-type Nir2, the extent of PIP_2 replenishment after receptor stimulation was reduced in cells overexpressing Nir2-FM (Figure 5G). These results suggest that Nir2 recruitment to ER-PM junctions following receptor stimulation is important for PM PIP_2 replenishment.

Enhanced ER-to-PM Connection by E-Syt1 Facilitates Nir2 Translocation to ER-PM Junctions

Next, we tested a hypothesis that the enhanced ER-to-PM connection by E-Syt1 contributes to Nir2 translocation to ER-PM junctions following receptor stimulation. Nir2 translocation to ER-PM junctions occurred quickly after histamine stimulation in siControl-transfected cells (Figure 6A). In contrast, aborted cycles of Nir2-mCherry translocation were observed in cells treated with siE-Syt1, in which the enhanced ER-to-PM connection failed to occur (Figures 3A and 3B). As a result, the maximal fold increase of Nir2-mCherry intensity at single ER-PM junctions was significantly reduced in siE-Syt1-transfected cells (Figure 6B). These results implicate that enhanced ER-to-PM connection mediated by E-Syt1 facilitates Nir2 translocation to ER-PM junctions after receptor stimulation.

To confirm that the enhanced ER-to-PM connection is important for Nir2 translocation, we applied MAPPER-s to restrict the range of gap distance of ER-PM junctions. Nir2 translocation was monitored in cells without overexpressing H1 receptor to

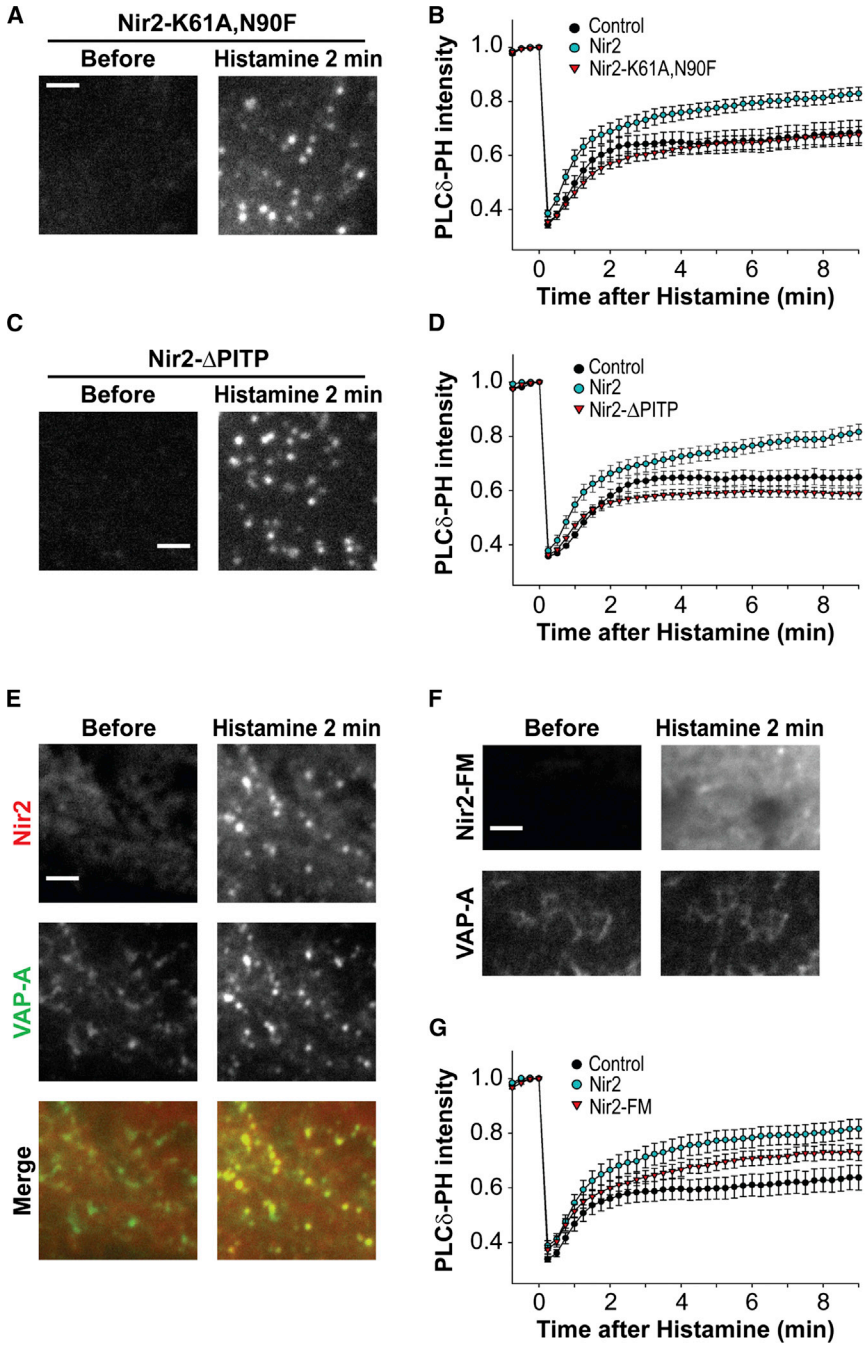

Figure 5. PI Transfer Activity and Targeting to ER-PM Junctions Are Important for Nir2 to Promote PIP_2 Replenishment following Receptor Stimulation

(A) Nir2-K61A,N90F mutant translocation induced by 100 μM histamine monitored by TIRF microscopy in HeLa cells cotransfected with H1 receptor and Nir2-K61A,N90F-mCherry. The scale bar represents 2 μm. See also Figure S7B.

(B) Dynamic changes of PLCδ-PH intensity induced by 100 μM histamine monitored by TIRF microscopy in HeLa cells cotransfected with H1 receptor, GFP-PLCδ-PH, and control, Nir2-mCherry or Nir2-K61A,N90F-mCherry. Mean ± SEM is shown (18–27 cells from three independent experiments). See also Figure S7C.

(C) Nir2-ΔPITP mutant translocation induced by 100 μM histamine monitored by TIRF microscopy in HeLa cells cotransfected with H1 receptor and Nir2-ΔPITP-mCherry. The scale bar represents 2 μm.

(D) Dynamic changes of PLCδ-PH intensity induced by 100 μM histamine monitored by TIRF microscopy in HeLa cells cotransfected with H1 receptor, GFP-PLCδ-PH, and control, Nir2-mCherry or Nir2-ΔPITP-mCherry. Mean ± SEM is shown (14–32 cells from three independent experiments).

(E and F) VAP-A and Nir2 or Nir2-FM (FFAT mutant) translocation induced by 100 μM histamine monitored by TIRF microscopy in HeLa cells cotransfected with H1 receptor, VAP-A-YFP, and Nir2-mCherry (E) or Nir2-FM-mCherry (F). The scale bar represents 2 μm. See also Figures S7D and S7E.

(G) Dynamic changes of PLCδ-PH intensity induced by 100 μM histamine monitored by TIRF microscopy in HeLa cells cotransfected with H1 receptor, GFP-PLCδ-PH, and control, Nir2-mCherry or Nir2-FM-mCherry. Mean ± SEM are shown (13–18 cells from three independent experiments).

demonstrate the enhancing effect of MAPPER-s. In MAPPER-expressing cells, histamine stimulation induced a weak translocation of Nir2, which was greatly potentiated in cells expressing MAPPER-s (Figure 6C). Further analyses showed that histamine stimulation induced a significantly higher increase of Nir2-mCherry intensity at ER-PM junctions in MAPPER-s-transfected cells than in MAPPER-transfected cells (Figure 6D). These results suggest that the gap distance of ER-PM junctions affects Nir2 translocation to ER-PM junctions following receptor stimulation.

Enhanced ER-to-PM Connection Promotes PIP_2 Replenishment and Supports Receptor-Induced Ca^{2+} Signaling

Because the enhanced ER-to-PM connection mediated by E-Syt1 is important for Nir2 translocation to ER-PM junctions, we tested the effect of *E-Syt1* knockdown on PM PIP_2 replenishment after receptor-induced hydrolysis. PM PIP_2 replenishment was markedly reduced in cells transfected with siE-Syt1_3′ UTR compared to that in siControl-transfected cells following histamine stimulation (Figure 6E). These results are consistent with the defective Nir2 translocation in siE-Syt1-treated cells. Expression of wild-type, but not the D724A mutant of E-Syt1 rescued the defective PM PIP_2 replenishment in *E-Syt1* knockdown cells (Figure 6E). These data indicate that E-Syt1 translocation to ER-PM junctions is crucial for replenishing PM PIP_2 after receptor-induced

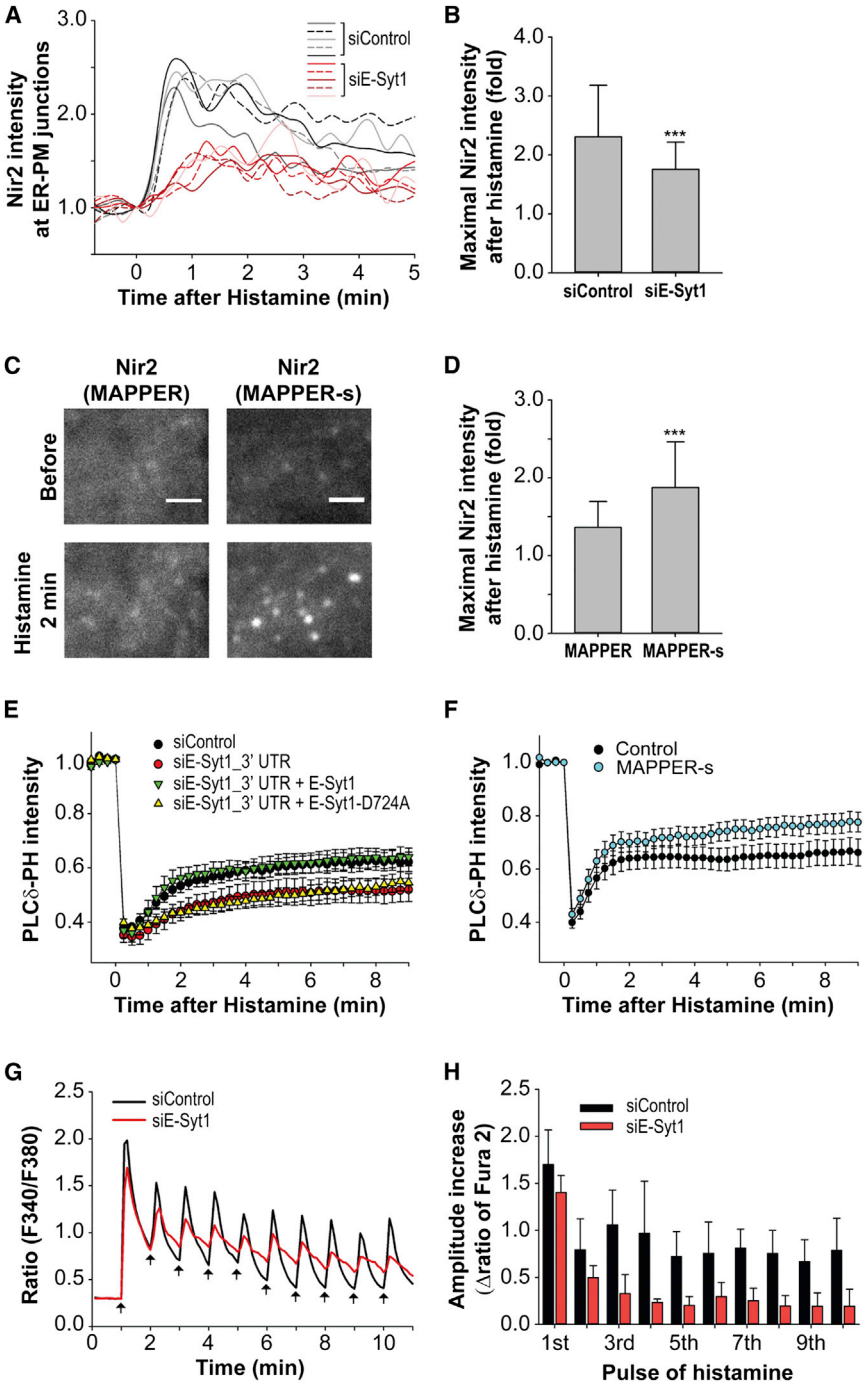

Figure 6. Enhancement of ER-to-PM Connection by E-Syt1 Facilitates Nir2 Translocation and PIP_2 Replenishment following Receptor Stimulation

(A) Nir2 accumulation at single ER-PM junctions induced by 100 μM histamine monitored by TIRF microscopy in HeLa cells cotransfected with H1 receptor, Nir2-mCherry, and siControl or siE-Syt1. Representative traces of Nir2 intensities at single ER-PM junctions are shown.

(B) Quantification of maximal fold increase of Nir2 intensities at single ER-PM junctions monitored as described in (A). Mean ± SD is shown (more than 250 puncta from two independent experiments). Triple asterisks denote $p < 0.001$.

(C) Nir2 translocation to ER-PM junctions induced by 100 μM histamine monitored by TIRF microscopy in HeLa cells cotransfected with Nir2-mCherry and MAPPER or MAPPER-s. The scale bar represents 2 μm.

(D) Quantification of maximal fold increase of Nir2 intensity at single ER-PM junctions monitored as described in (C). Mean ± SD is shown (more than 60 puncta). Triple asterisks denote $p < 0.001$.

(E) Dynamic changes of PLCδ-PH intensities induced by 100 μM histamine monitored by TIRF microscopy in HeLa cells cotransfected with H1 receptor, GFP-PLCδ-PH, siControl or siE-Syt1, plus mCherry-E-Syt1 or mCherry-E-Syt1-D724A. Mean ± SEM is shown (five to nine cells from three independent experiments).

(F) Dynamic changes of PLCδ-PH intensities induced by 100 μM histamine monitored by TIRF microscopy in HeLa cells cotransfected with H1 receptor, mCherry-PLCδ-PH, and control (SP-GFP-TM) or MAPPER-s. Mean ± SEM are shown (13–14 cells from two independent experiments).

(G) Relative changes in cytosolic Ca^{2+} concentration monitored by Fura2 ratio in HeLa cells cotransfected with H1 receptor and siControl or siE-Syt1. Cells were subjected to multiple pulses of 100 μM histamine treatment (arrows) in a perfusion system providing a constant flow of ECB. Average traces are shown (four wells from two independent experiments; each well contained at least 300 cells).

(H) Quantification of amplitude increases of each pulse from data shown in (G). Mean ± SD is shown (four wells from two independent experiments).

hydrolysis. Consistently, we observed that expression of MAPPER-s, which restricts the range of gap distance of ER-PM junctions, promoted PM PIP_2 replenishment after hydrolysis (Figure 6F). Together, these results suggest that the enhanced ER-to-PM connection induced by E-Syt1 translocation to ER-PM junctions is essential for replenishing PM PIP_2 after receptor stimulation.

It is likely that defective PM PIP_2 replenishment after receptor-induced hydrolysis affects the ability of cells to respond to subsequent stimulation. To test this hypothesis, we monitored Ca^{2+} signaling responses induced by periodic treatment of histamine. We observed that the first and second pulses of histamine stimulation triggered comparable amplitude increases in Ca^{2+} responses in siControl- and siE-Syt1-transfected cells (Figures 6G and 6H). Strikingly, a profound decrease in amplitude of Ca^{2+} responses to subsequent histamine pulses was observed in siE-Syt1-transfected cells. These results suggest that the enhanced ER-to-PM connection and PM PIP_2 replenishment are important for the recovery of the Ca^{2+} signaling system following receptor stimulation.

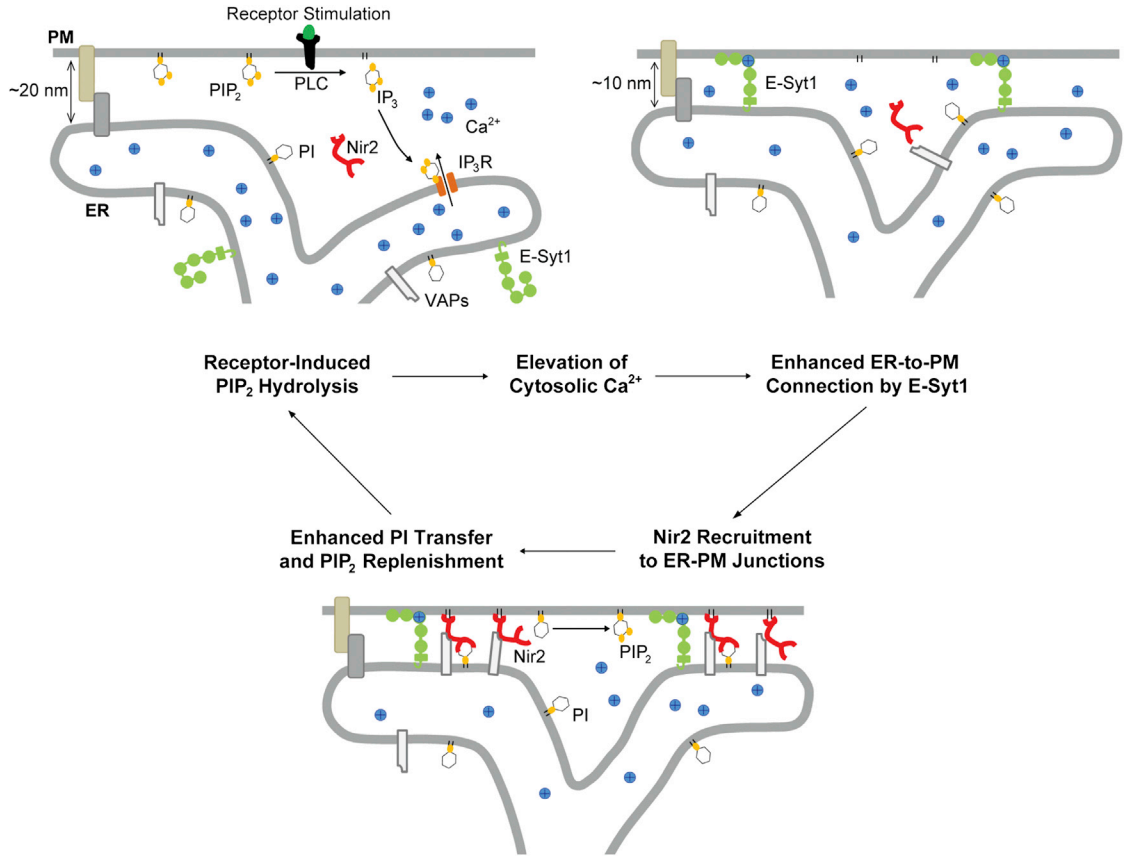

Figure 7. Model of a Feedback Mechanism for Receptor-Induced Ca^{2+} Signaling

Stimulation of numerous receptors activates PLC, which hydrolyzes PIP_2 at the PM to produce IP_3. IP_3 triggers a release of ER Ca^{2+} and an increase in cytosolic Ca^{2+}. Subsequently, E-Syt1 binds Ca^{2+} and translocates to ER-PM junctions to induce new junction formation and a decrease in gap distance between the ER and the PM. Enhancement of ER-to-PM connection induced by E-Syt1 facilitates Nir2 recruitment to ER-PM junctions and PI transfer from the ER to the PM. PI is then converted to PIP_2 at the PM to support receptor-induced Ca^{2+} signaling.

DISCUSSION

Based on our findings, we propose a model of a feedback mechanism for receptor-induced Ca^{2+} signaling (Figure 7). Stimulation of many cell surface receptors leads to the activation of PLC. Activated PLC hydrolyzes PIP_2 at the PM to produce IP_3 that induces a release of ER Ca^{2+} to the cytosol through IP_3 receptors. Our study indicates that E-Syt1 binds Ca^{2+} in response to elevation of cytosolic Ca^{2+} and translocates to ER-PM junctions, triggering an enhanced connection between the ER and the PM. This enhanced ER-to-PM connection facilitates Nir2 recruitment to ER-PM junctions. At these junctions, Nir2 may efficiently transfer PI synthesized in the ER to the PM for a subsequent conversion to PIP_2 to support receptor-induced Ca^{2+} signaling. In this model, elevation of cytosolic Ca^{2+} resulting from PIP_2 hydrolysis, enhanced ER-to-PM connection mediated by the Ca^{2+} effector E-Syt1, recruitment of Nir2 to ER-PM junctions, and PM PIP_2 replenishment via Nir2 constitute a feedback mechanism to replenish PM PIP_2 after initial receptor activation and to prepare the signaling system for additional stimulation.

By generating MAPPER, a marker that contains minimal ER- and PM-targeting motifs, a fluorescent protein, and several rigid and flexible linkers in the cytosolic region setting the proper gap distance, we successfully labeled ER-PM junctions in live mammalian cells without significantly affecting their size, density, and functions. Several methods have been developed previously for visualizing or manipulating ER-PM junctions in yeast and in mammalian cells (Ercan et al., 2009; Lavieu et al., 2010; Várnai et al., 2007; Zhang et al., 2012). Our method minimizes cell perturbations and can be easily applied to track dynamic changes and biological processes occurring at ER-PM junctions. Using MAPPER and high-resolution TIRF microscopy, we demonstrated that changes in cytosolic Ca^{2+} levels dynamically regulate ER-PM junctions. In addition to new junction formation, our data suggest that a decrease in gap distance of ER-PM junctions occurs following elevation of cytosolic Ca^{2+}. The dynamic regulation of gap distance of ER-PM junctions by cytosolic Ca^{2+} levels may have important functional consequences. It is plausible that changes in gap distance exclude certain proteins while recruiting others, such as Nir2, to ER-PM junctions. Therefore, modulating the gap of ER-PM junctions by signaling inputs may switch cellular functions on or off at these sites.

The translocation of Nir2 from the cytosol to ER-PM junctions suggests that it binds to the ER and the PM simultaneously

following receptor stimulation. Our results and others demonstrate that Nir2 interacts with the ER membrane protein VAP-A and VAP-B via its FFAT motif (Amarilio et al., 2005). Concentration of VAPs to ER-PM junctions by Nir2 may further recruit other FFAT-motif-containing proteins to mediate additional cellular functions (Lev et al., 2008). The PM-targeting mechanism of Nir2 is unclear. It is plausible that the PM-binding partner of Nir2 is generated by receptor activation because the extent of histamine-induced Nir2 translocation was strongly enhanced in cells overexpressing H1 receptor. Moreover, we show that Nir2 recruitment to ER-PM junctions is dependent on an enhanced ER-to-PM connection. We propose that the recruitment of Nir2 to ER-PM junctions during receptor-induced Ca^{2+} signaling requires that three events occur concurrently: (1) Nir2 interaction with VAPs in the ER membrane; (2) Nir2 PM targeting; and (3) a decrease in gap distance of ER-PM junctions induced by increases in cytosolic Ca^{2+}. These events may serve as gates to prevent Nir2 translocation by cytosolic Ca^{2+} fluctuation without receptor activation. In addition, these gates may ensure that PIP_2 replenishment occurs at ER-PM junctions near the subcellular loci of receptor-induced hydrolysis. PM PIP_2 is important for many cellular functions, such as endocytosis and regulation of the actin cytoskeleton (Di Paolo and De Camilli, 2006). Therefore, further investigation of Nir2 PM-targeting mechanisms may have a broad impact on PM PIP_2-regulated cellular functions.

Our data reveal a critical role of Nir2 in replenishing PM PIP_2 following receptor stimulation. It was proposed many years ago that lipid transfer proteins may mediate a cycle of PI metabolism between the ER and the PM induced by receptor stimulation (Michell, 1975). In addition, it has been suggested that the PITP RdgB may transfer PI from the ER to the PM at ER-PM junctions to sustain receptor functions in *Drosophila* photoreceptor cells (Carrasco and Meyer, 2011; Levine, 2004). In this report, we provide evidence supporting these hypotheses by showing that Nir2, a mammalian ortholog of RdgB, translocates to ER-PM junctions and promotes PM PIP_2 replenishment during receptor-induced Ca^{2+} signaling. It is likely that Nir2 mediates PM PIP_2 replenishment by transferring PI from the ER to the PM at ER-PM junctions, which may work synergistically with other PI-transferring mechanisms, including PI delivery by a highly mobile ER-derived PI-synthesizing compartment that makes repetitive contacts with other organelles (Kim et al., 2011). It is also possible that Nir2 modulates PM PIP_2 levels by mechanisms other than transferring PI from the ER to the PM, such as presenting PI from the ER and/or the PM to kinases on the PM (Schaaf et al., 2008) or activating enzymes that regulate phosphoinositide metabolism at ER-PM junctions (Stefan et al., 2011). Additional work is needed to test these possibilities.

Feedback loops connect output signals to their original inputs and are important for maintaining cellular homeostasis (Brandman and Meyer, 2008). Our results indicate a feedback mechanism that connects cytosolic Ca^{2+} signals originating from receptor-induced PM PIP_2 hydrolysis back to the PM by PIP_2 replenishment via E-Syt1 and Nir2 at ER-PM junctions. Overall, our findings provide mechanistic insights into the crosstalk between Ca^{2+} signaling and PIP_2 metabolism at ER-PM junctions.

EXPERIMENTAL PROCEDURES

Reagents

TG, Pluronic F-127, BAPTA-AM, NP-EGTA, and Fura-2 AM were purchased from Invitrogen. All chemicals for extracellular buffer (ECB, 125 mM NaCl, 5 mM KCl, 1.5 mM $MgCl_2$, 20 mM HEPES, 10 mM glucose, and 1.5 mM $CaCl_2$ [pH 7.4]), 100X penicillin and streptomycin solutions, histamine, and EGTA were obtained from Sigma. siRNAs used in this study were generated as described previously (Liou et al., 2005). Primers used for siRNA generation are listed in Table S1.

Cell Culture and Transfection

HeLa cells purchased from American Type Culture Collection were cultured in minimum essential medium supplemented with 10% fetal bovine serum (HyClone) and 1X penicillin and streptomycin solution. DNA plasmids (15–50 ng) and siRNAs (10–25 nM) were transfected into HeLa cells with TransIT-LT1 reagent and TransIT-TKO reagent, respectively (Muris).

DNA Constructs

mCherry-tagged human STIM1 (SP-mCherry-STIM1) was constructed by replacing the cyan fluorescent protein (CFP) portion of SP-CFP-STIM1 (Liou et al., 2005) with mCherry. Orai1-mCherry was constructed by replacing the yellow fluorescent protein (YFP) portion of Orai1-YFP (Várnai et al., 2007) with mCherry. mCherry-ER was constructed by replacing the sequence of STIM1 from SP-mCherry-STIM1 with oligonucleotides containing the coding sequence of KDEL and a stop codon. YFP-ER was described previously (Liou et al., 2005). mCherry-E-Syt1 was cloned by replacing the KDEL portion of mCherry-ER with a PCR fragment encoding amino acid 53-1104 of E-Syt1 transcript 2 (NM_015292). E-Syt1-mCherry and Nir2-mCherry were cloned by replacing the Orai1 part of Orai1-mCherry with PCR fragments of full-length E-Syt1 or full-length Nir2, respectively. Both mCherry-E-Syt1 and E-Syt1-mCherry were cloned using In-Fusion-HD cloning kit (Clontech Laboratories). Mutants of E-Syt1 and Nir2 were generated using QuickChange site-direct mutagenesis kit (Agilent Technologies) with oligonucleotides containing mutated coding sequences. mCherry-PLCδ-PH was constructed by replacing the GFP part of GFP-PLCδ-PH with mCherry. VAP-A-YFP and VAP-B-YFP were cloned by inserting PCR fragments containing full-length VAP-A and VAP-B into YFP-N1. All constructs listed here were verified by sequencing. All oligonucleotides used in this study are listed in Table S1. Details for MAPPER-s and MAPPER construction are in the Supplemental Experimental Procedures.

Electron Microscopy

miniSOG-MAPPER was revealed by EM following the method of Shu et al. (2011) with modifications. Additional details are in the Supplemental Experimental Procedures.

Live-Cell Confocal and TIRF Microscopy

HeLa cells were cultured on Lab-Tek chambered cover glass (NUNC). Before imaging, cells were washed with ECB. Live-cell confocal and TIRF imaging experiments were performed at room temperature with 60× or 100× objectives and a custom-built confocal-TIRF microscope controlled by Micro-Manager software (Edelstein et al., 2010). In order to manipulate intracellular Ca^{2+} levels, cells were loaded with 10 μM BAPTA-AM or 20 μM NP-EGTA in ECB containing 0.05% Pluronic F-127 and 0.1% of BSA at room temperature for 30 min. Loaded cells were then washed twice with ECB containing 0.1% BSA and incubated in ECB for another 15–30 min before the experiments. To release Ca^{2+} from NP-EGTA, cells were exposed to a 405 nm laser pulse for 400–800 ms at rates of 6 s or 10 s per frame. The PM PIP_2 level was determined by the intensity of GFP-PLCδ-PH, mCherry-PLCδ-PH, or Tubby-GFP using TIRF microscopy, and an ND8 filter was introduced to the light path to prevent photobleaching. Details for image analyses are in the Supplemental Experimental Procedures.

Ca^{2+} Measurements

Cytosolic Ca^{2+} levels were measured as described previously (Liou et al., 2005). For periodic histamine stimulation experiments, Fura-2-loaded cells were placed in a perfusion system built in the lab providing a constant ECB

flow of 1.5–2 ml per min. Histamine (100 μM) was added every minute. Additional details are in the Supplemental Experimental Procedures.

Statistical Analyses

Data were analyzed by a Student's t test or one-way ANOVA with SigmaPlot (Systat Software).

SUPPLEMENTAL INFORMATION

Supplemental Information includes Supplemental Experimental Procedures, seven figures, one table, and six movies and can be found with this article online at http://dx.doi.org/10.1016/j.celrep.2013.09.038.

AUTHOR CONTRIBUTIONS

J.L. and C.-L.C. designed MAPPER. C.-L.C. performed all experiments except EM and STED microscopy. C.-L.C., T.-S.H., and J.L. analyzed the results. T.T.Y. and J.-C.L. performed STED microscopy and STED image analysis. K.G.R. performed EM experiments. C.-L.C., D.B.A., and E.V. generated constructs. J.L. conceived and supervised the project. J.L. and C.-L.C. wrote the manuscript.

ACKNOWLEDGMENTS

We are grateful to Dr. Katherine Luby-Phelps at the UT Southwestern Live-Cell Imaging Facility for assistance with electron microscopy and advice, Dr. Elliott Ross for providing histamine H1 receptor plasmid, Dr. Robert Campbell for providing R-GECO1 and GEM-GECO1 plasmids, Dr. Roger Tsien for providing miniSOG plasmids, Dr. Tobias Meyer for providing YFP-Rit tail and GFP-PLCδ-PH plasmids, Dr. Richard Lewis for providing FRB-STIM1 plasmid, Dr. Tamas Balla for providing Orai1-YFP plasmid, Dr. Andrew Tinker for providing Tubby-GFP plasmid, and Linda Patterson for administrative assistance. We thank Dr. James Stull, Dr. Helen Yin, and Dr. Ilya Bezprozvanny for comments on the manuscript. J.L. is a Sowell Family Scholar in Medical Research. This work was supported by Welch Foundation grant I-1789. T.T.Y. and J.-C.L. are supported by NSF grant CMMI-1125760.

Received: June 28, 2013
Revised: September 6, 2013
Accepted: September 25, 2013
Published: October 31, 2013

REFERENCES

Aikawa, Y., Kuraoka, A., Kondo, H., Kawabuchi, M., and Watanabe, T. (1999). Involvement of PITPnm, a mammalian homologue of Drosophila rdgB, in phosphoinositide synthesis on Golgi membranes. J. Biol. Chem. *274*, 20569–20577.

Amarilio, R., Ramachandran, S., Sabanay, H., and Lev, S. (2005). Differential regulation of endoplasmic reticulum structure through VAP-Nir protein interaction. J. Biol. Chem. *280*, 5934–5944.

Berridge, M.J., Lipp, P., and Bootman, M.D. (2000). The versatility and universality of calcium signalling. Nat. Rev. Mol. Cell Biol. *1*, 11–21.

Brandman, O., and Meyer, T. (2008). Feedback loops shape cellular signals in space and time. Science *322*, 390–395.

Carrasco, S., and Meyer, T. (2011). STIM proteins and the endoplasmic reticulum-plasma membrane junctions. Annu. Rev. Biochem. *80*, 973–1000.

Cockcroft, S. (2012). The diverse functions of phosphatidylinositol transfer proteins. Curr. Top. Microbiol. Immunol. *362*, 185–208.

Di Paolo, G., and De Camilli, P. (2006). Phosphoinositides in cell regulation and membrane dynamics. Nature *443*, 651–657.

Edelstein, A., Amodaj, N., Hoover, K., Vale, R., and Stuurman, N. (2010). Computer control of microscopes using μManager. Curr. Protoc Mo. Biol. *Chapter 14*, Unit14.20.

Ercan, E., Momburg, F., Engel, U., Temmerman, K., Nickel, W., and Seedorf, M. (2009). A conserved, lipid-mediated sorting mechanism of yeast Ist2 and mammalian STIM proteins to the peripheral ER. Traffic *10*, 1802–1818.

Friedman, J.R., and Voeltz, G.K. (2011). The ER in 3D: a multifunctional dynamic membrane network. Trends Cell Biol. *21*, 709–717.

Giordano, F., Saheki, Y., Idevall-Hagren, O., Colombo, S.F., Pirruccello, M., Milosevic, I., Gracheva, E.O., Bagriantsev, S.N., Borgese, N., and De Camilli, P. (2013). PI(4,5)P(2)-dependent and Ca(2+)-regulated ER-PM interactions mediated by the extended synaptotagmins. Cell *153*, 1494–1509.

Heo, W.D., Inoue, T., Park, W.S., Kim, M.L., Park, B.O., Wandless, T.J., and Meyer, T. (2006). PI(3,4,5)P3 and PI(4,5)P2 lipids target proteins with polybasic clusters to the plasma membrane. Science *314*, 1458–1461.

Kim, Y.J., Guzman-Hernandez, M.L., and Balla, T. (2011). A highly dynamic ER-derived phosphatidylinositol-synthesizing organelle supplies phosphoinositides to cellular membranes. Dev. Cell *21*, 813–824.

Korzeniowski, M.K., Popovic, M.A., Szentpetery, Z., Varnai, P., Stojilkovic, S.S., and Balla, T. (2009). Dependence of STIM1/Orai1-mediated calcium entry on plasma membrane phosphoinositides. J. Biol. Chem. *284*, 21027–21035.

Lavieu, G., Orci, L., Shi, L., Geiling, M., Ravazzola, M., Wieland, F., Cosson, P., and Rothman, J.E. (2010). Induction of cortical endoplasmic reticulum by dimerization of a coatomer-binding peptide anchored to endoplasmic reticulum membranes. Proc. Natl. Acad. Sci. USA *107*, 6876–6881.

Lev, S., Ben Halevy, D., Peretti, D., and Dahan, N. (2008). The VAP protein family: from cellular functions to motor neuron disease. Trends Cell Biol. *18*, 282–290.

Levine, T. (2004). Short-range intracellular trafficking of small molecules across endoplasmic reticulum junctions. Trends Cell Biol. *14*, 483–490.

Lewis, R.S. (2011). Store-operated calcium channels: new perspectives on mechanism and function. Cold Spring Harb. Perspect. Biol. *3*, pii: a003970.

Liou, J., Kim, M.L., Heo, W.D., Jones, J.T., Myers, J.W., Ferrell, J.E., Jr., and Meyer, T. (2005). STIM is a Ca2+ sensor essential for Ca2+-store-depletion-triggered Ca2+ influx. Curr. Biol. *15*, 1235–1241.

Liou, J., Fivaz, M., Inoue, T., and Meyer, T. (2007). Live-cell imaging reveals sequential oligomerization and local plasma membrane targeting of stromal interaction molecule 1 after Ca2+ store depletion. Proc. Natl. Acad. Sci. USA *104*, 9301–9306.

Manford, A.G., Stefan, C.J., Yuan, H.L., Macgurn, J.A., and Emr, S.D. (2012). ER-to-plasma membrane tethering proteins regulate cell signaling and ER morphology. Dev. Cell *23*, 1129–1140.

Michell, R.H. (1975). Inositol phospholipids and cell surface receptor function. Biochim. Biophys. Acta *415*, 81–47.

Min, S.W., Chang, W.P., and Südhof, T.C. (2007). E-Syts, a family of membranous Ca2+-sensor proteins with multiple C2 domains. Proc. Natl. Acad. Sci. USA *104*, 3823–3828.

Orci, L., Ravazzola, M., Le Coadic, M., Shen, W.W., Demaurex, N., and Cosson, P. (2009). From the Cover: STIM1-induced precortical and cortical subdomains of the endoplasmic reticulum. Proc. Natl. Acad. Sci. USA *106*, 19358–19362.

Putyrski, M., and Schultz, C. (2012). Protein translocation as a tool: The current rapamycin story. FEBS Lett. *586*, 2097–2105.

Quinn, K.V., Behe, P., and Tinker, A. (2008). Monitoring changes in membrane phosphatidylinositol 4,5-bisphosphate in living cells using a domain from the transcription factor tubby. J. Physiol. *586*, 2855–2871.

Schaaf, G., Ortlund, E.A., Tyeryar, K.R., Mousley, C.J., Ile, K.E., Garrett, T.A., Ren, J., Woolls, M.J., Raetz, C.R., Redinbo, M.R., and Bankaitis, V.A. (2008). Functional anatomy of phospholipid binding and regulation of phosphoinositide homeostasis by proteins of the sec14 superfamily. Mol. Cell *29*, 191–206.

Shu, X., Lev-Ram, V., Deerinck, T.J., Qi, Y., Ramko, E.B., Davidson, M.W., Jin, Y., Ellisman, M.H., and Tsien, R.Y. (2011). A genetically encoded tag for correlated light and electron microscopy of intact cells, tissues, and organisms. PLoS Biol. *9*, e1001041.

Stauffer, T.P., Ahn, S., and Meyer, T. (1998). Receptor-induced transient reduction in plasma membrane PtdIns(4,5)P2 concentration monitored in living cells. Curr. Biol. *8*, 343–346.

Stefan, C.J., Manford, A.G., Baird, D., Yamada-Hanff, J., Mao, Y., and Emr, S.D. (2011). Osh proteins regulate phosphoinositide metabolism at ER-plasma membrane contact sites. Cell *144*, 389–401.

Steyer, J.A., and Almers, W. (2001). A real-time view of life within 100 nm of the plasma membrane. Nat. Rev. Mol. Cell Biol. *2*, 268–275.

Toulmay, A., and Prinz, W.A. (2011). Lipid transfer and signaling at organelle contact sites: the tip of the iceberg. Curr. Opin. Cell Biol. *23*, 458–463.

Toulmay, A., and Prinz, W.A. (2012). A conserved membrane-binding domain targets proteins to organelle contact sites. J. Cell Sci. *125*, 49–58.

Várnai, P., Tóth, B., Tóth, D.J., Hunyady, L., and Balla, T. (2007). Visualization and manipulation of plasma membrane-endoplasmic reticulum contact sites indicates the presence of additional molecular components within the STIM1-Orai1 Complex. J. Biol. Chem. *282*, 29678–29690.

Vihtelic, T.S., Goebl, M., Milligan, S., O'Tousa, J.E., and Hyde, D.R. (1993). Localization of Drosophila retinal degeneration B, a membrane-associated phosphatidylinositol transfer protein. J. Cell Biol. *122*, 1013–1022.

Walsh, C.M., Chvanov, M., Haynes, L.P., Petersen, O.H., Tepikin, A.V., and Burgoyne, R.D. (2010). Role of phosphoinositides in STIM1 dynamics and store-operated calcium entry. Biochem. J. *425*, 159–168.

Willig, K.I., Kellner, R.R., Medda, R., Hein, B., Jakobs, S., and Hell, S.W. (2006). Nanoscale resolution in GFP-based microscopy. Nat. Methods *3*, 721–723.

Wu, M.M., Buchanan, J., Luik, R.M., and Lewis, R.S. (2006). Ca2+ store depletion causes STIM1 to accumulate in ER regions closely associated with the plasma membrane. J. Cell Biol. *174*, 803–813.

Zhang, D., Vjestica, A., and Oliferenko, S. (2012). Plasma membrane tethering of the cortical ER necessitates its finely reticulated architecture. Curr. Biol. *22*, 2048–2052.

Zhao, Y., Araki, S., Wu, J., Teramoto, T., Chang, Y.F., Nakano, M., Abdelfattah, A.S., Fujiwara, M., Ishihara, T., Nagai, T., and Campbell, R.E. (2011). An expanded palette of genetically encoded Ca^{2+} indicators. Science *333*, 1888–1891.